ORIGINAL PAPER

New insights into the high-pressure polymorphism of SiO_2 cristobalite

Przemyslaw Dera · John D. Lazarz ·
Vitali B. Prakapenka · Madison Barkley ·
Robert T. Downs

Abstract Single-crystal X-ray diffraction experiments with SiO_2 α-cristobalite reveal that the well-known reversible displacive phase transition to cristobalite-II, which occurs at approximately 1.8 GPa, can be suppressed by rapid pressure increase, leading to an overpressurized metastable state, persisting to pressure as high as 10 GPa. In another, slow pressure increase experiment, the monoclinic high-pressure phase-II was observed to form at ∼1.8 GPa, in agreement with earlier in situ studies, and its crystal structure has been unambiguously determined. Single-crystal data have been used to refine the structure models of both phases over the range of pressure up to the threshold of formation of cristobalite X-I at ∼12 GPa, providing important constraints on the feasibility of the two competing silica densification models proposed in the literature, based on quantum mechanical calculations. Preliminary diffraction data obtained for cristobalite X-I reveal a monoclinic unit cell that contradicts the currently assumed model.

Keywords High pressure · Phase transitions · Metastability · Polymorphism · Silica

P. Dera (✉) · J. D. Lazarz · V. B. Prakapenka
Center for Advanced Radiation Sources,
The University of Chicago, Argonne National Laboratory,
Building 434A, 9700 South Cass Ave, Argonne, IL 60439, USA
e-mail: dera@cars.uchicago.edu

M. Barkley · R. T. Downs
Department of Geosciences, University of Arizona,
Tucson, AZ 85721-0077, USA

Introduction

Silicon dioxide SiO_2 is not only one of the most common natural chemical compounds found both on the surface as well as in the interior of the Earth, but also plays a very important role in many technological and industrial applications. Despite the simple chemical composition, SiO_2 exhibits a rather rich and complicated behavior in response to variations in thermodynamic conditions. Our understanding of the phase relations of SiO_2 in pressure–temperature space is complicated by numerous examples of metastability and path-dependent phase transition sequences. The origin of this behavior in the tetrahedral silicate phases is generally attributed to the interplay between strong SiO_4 tetrahedral groups and weak Si–O–Si linkages (Downs and Palmer 1994). Among the several crystalline polymorphs of silica that are stable or metastable at ambient conditions, the most widely known are quartz, coesite, cristobalite, and tridymite, with the latter two being high-temperature phases. Stishovite is the well-studied silica phase with SiO_6 octahedra. In addition to the variety of crystalline phases, amorphous silica glass is also commonly found in natural geologic environments and utilized in technology. The general tendency observed during compression of SiO_2 is that the low-pressure, tetrahedrally coordinated polymorphs transform to octahedrally coordinated phases, such as stishovite, accompanied by a significant increase in density (densification). The exact value of pressure for the 4–6 transformation as well as the transition mechanism (pathway through intermediate phases) is strongly dependent on the initial polymorph, as well as factors such as stress anisotropy. Cristobalite has been one of the most widely studied SiO_2 phases. The tetragonal α-phase is usually metastably quenched as twinned crystals from the cubic β-cristobalite that is stable above 1,470°C, can be found in

natural acidic volcanic rocks, and is one of the major components of precious opal. However, the sample used in this study formed as untwined crystals at low temperatures directly as α-cristobalite onto mordenite crystals that appear to have acted as templates for their growth (Van Valkenburg and Buie 1945).

All of the previously published results of static compression experiments with the tetragonal α-cristobalite indicate that at pressure of approximately 1.8 GPa, a reversible, displacive first-order phase transition occurs, which leads to the formation of monoclinic cristobalite-II (Downs and Palmer 1994; Palmer and Finger 1994; Palmer et al. 1994; Onodera et al. 1997). The structure of this phase was initially elusive, until a neutron powder diffraction experiment combined with theoretical modeling yielded a model with space group $P2_1/c$ (Dove et al. 2000). On further compression at approximately 12 GPa, the monoclinic structure transforms to another phase, known as cristobalite X-I (e.g., Palmer et al. 1994).

The recent decade witnessed a wealth of ab initio studies aimed at modeling the high-pressure transformations of cristobalite, which paint a rather complex and not very uniform picture of the phase diagram and transformation sequences, and are often in disagreement with experiments. Huang et al. (2006) predicted that the α-phase is stable to 15 GPa and then transforms first to an orthorhombic $C222_1$ polymorph (different than the monoclinic cristobalite-II) stable between 15 and 18 GPa, and then to new tetrahedral phase with tetragonal $P4_12_12$ symmetry (the same as in α-cristobalite). One of the most important conclusions of this study was a hypothesis suggesting that the transformation from tetrahedral to octahedrally coordinated silica should occur through a continuous rearrangement of the oxygen sublattice within the tetrahedral phase from body-centered cubic (bcc) toward hexagonal closed packed (hcp), which would be in contrast to the trend observed in experiments with quartz (Thompson and Downs 2010). On further simulated compression, the $P4_12_12$ phase transformed to stishovite at 22 GPa. A direct α-cristobalite to tetragonal phase transition was found in the first principles molecular dynamics study by Donadio et al. (2008). Liang et al. (2007), on the other hand, obtained results from nonhydrostatic molecular dynamics simulations, suggesting that the oxygen sublattice transformation and formation of the octahedrally coordinated phase are achieved in one discontinuous step. These calculations also suggested formation of a tetrahedral $C222_1$ phase on decompression of a hypothetical intermediate, penta-coordinated phase with symmetry $P2_1$. Other quantum mechanical simulations, which considered anisotropic stress effects (Durandurdu 2009), suggest the possibility of yet another intermediate tetrahedral phase with symmetry $P2_12_12_1$.

One of the more interesting recent theoretical findings was a suggestion that the high-pressure transformation path in cristobalite may depend not only on the anisotropy of the stress field but also on the rate of compression. The classical molecular dynamics simulations of Garg and Sharma (2007) indicate that a transformation of α-cristobalite to the hypothetical $Cmcm$ phase, originally predicted by Tsenyuki et al. (1989) can be observed during compression involving small and gradual pressure increases, whereas it is completely suppressed if the pressure increase steps are as large as 5 GPa.

There is a clear need for detailed knowledge of the compression mechanisms of α-cristobalite and cristobalite-II. Without this knowledge, it is very difficult to reconcile the validity of the various theoretical predictions. Unfortunately, the compression mechanism of the α-phase has been established only to 1.6 GPa (Downs and Palmer 1994), because of the α → II phase transition, and for phase-II the structure has been refined only at one pressure point (Dove et al. 2000). Intrigued by the possibility that perhaps the prediction of the compression rate-induced suppression of the phase transitions (Garg and Sharma 2007) may extend to the α → II transformation as well, we decided to conduct a series of hydrostatic, synchrotron single-crystal X-ray diffraction experiments involving small and large pressure increases, aimed at elucidation of the detailed compression mechanisms of phases α and II.

Experimental

We performed two independent high-pressure diffraction experiments (S_1 and S_2) with untwined single-crystal samples from Ellora Caves, India (Harvard Mineralogical Museum 97849). These were the same crystals as used in earlier studies by the researchers from the Carnegie Institution of Washington. In each experiment, single-crystal specimens with different orientations (one crystal in S_1 and three crystals in S_2) were loaded into the diamond anvil cell (DAC). In both experiments, a symmetric piston-cylinder Princeton-type diamond anvil cell was used. Diamond anvils with culets of 0.3 mm were mounted on asymmetric backing plates (cubic boron nitride toward the X-ray source and tungsten carbide toward the detector). Rhenium metal gaskets preindented to 0.045 mm (experiment S_1) and 0.042 mm (experiment S_2) were used for sample containment. In experiment S_1, the DAC was loaded with 4:1 methanol–ethanol mixture, whereas in S_2 Ne pressure medium was loaded using the GSECARS/COMPRES gas loading system (Rivers et al. 2008). In both experiments, pressure was estimated based on a ruby fluorescence spectrum collected at each pressure point both before and after the X-ray data collection using the equation of Mao et al.
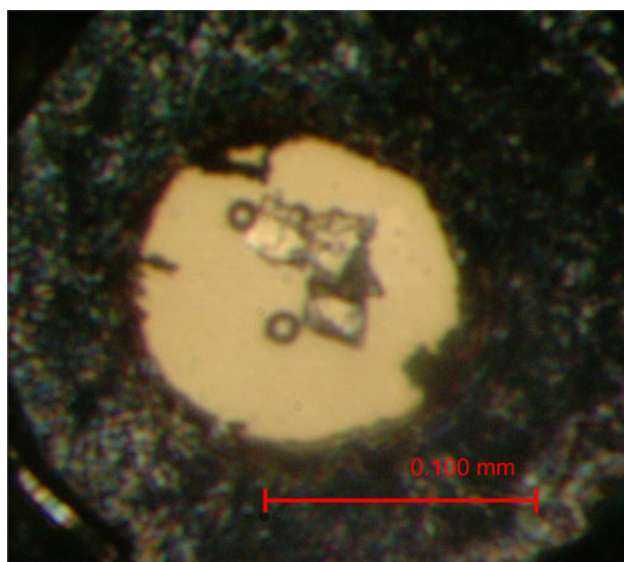
Fig. 1 Experiment S2: three single crystals of α-cristobalite in the diamond anvil cell after gas loading with Ne at pressure of 1.2(1) GPa. The diameter of the hole in the gasket is approximately 0.120 mm

(1986). In experiment S_2, in addition to the ruby pressure gauge, all pressure measurements above 5 GPa were estimated from the diffraction signal of solid Ne using the equation of state of Dewaele et al. (2008). Within the studied pressure range, both alcohol and Ne maintain an almost ideal hydrostaticity (Klotz et al. 2009), and our experimental data showed no indication of anisotropic stress. Figure 1 shows the three single-crystal specimens in experiment S_2 loaded into DAC at a pressure of 1.2(1) GPa.

Single-crystal X-ray diffraction data were collected at the experimental station 13IDD of the GSECARS facility at Advanced Photon Source, Argonne National Laboratory. A monochromatic beam with incident energy of 37 keV was focused with a pair of Kirkpatrick-Baez mirrors to a spot of 0.003 by 0.005 mm. Diffraction images were collected using a MAR165 charge-coupled device (CCD) detector, placed at a sample-to-detector distance of approximately 200 mm. During the exposure, the sample was rotated about the vertical axis of the instrument (ω) in the range of $\pm25°$ with a typical exposure time of 5 s for the full 50° rotation. Diffraction images were collected at three detector positions, differing by a translation of 70 mm perpendicular to the incident beam. In addition to the full-rotation exposures, a step-scan with 1° rotation steps was performed at each pressure step, for each of the crystals. Diffraction images were analyzed using the GSE_ADA/RSV software package (Dera 2007).

In experiment S_1, the pressure inside the DAC after closing the cell was 0.6(1) GPa, well below the $\alpha \rightarrow$ II transition. Diffraction data collected at this pressure (Fig. 2) could be successfully indexed using the tetragonal unit cell of the ambient α-phase. In order to test the feasibility of

metastable overpressurization[1], the pressure was then rapidly increased to 7.4(1) GPa in one step. The single-crystal diffraction image recorded at this pressure (Fig. 2) indeed showed only minor changes resulting from the compression-induced unit cell volume reduction, but clearly indicated preservation of the α-phase almost 6 GPa above the previously established phase boundary. Pressure was further increased to 9.1(1) GPa without any indication of the phase transition. Since the hydrostatic limit for the alcohol mixture pressure medium is approximately 10 GPa, we then collected data on decompression of the overpressurized metastable α-phase at 5.4(1) and 3.6(1) GPa.

In experiment S_2, the pressure inside the DAC after closing the cell was 1.2(1) GPa, and the diffraction images indicated the α-phase nature of all three single-crystal specimens. The pressure was then gradually increased in steps of not more than 0.5 GPa to 4.9(1) GPa. Diffraction data recorded at this pressure point showed clear evidence of a phase transition in all three specimens (Fig. 3). Diffraction patterns could be indexed based on a primitive monoclinic unit cell of cristobalite-II, equivalent to the one reported by Dove et al. (2000). Diffraction data for cristobalite-II were then collected at two more pressure steps of 7.3(1) and 10.1(1) GPa. A further pressure increase to 12.9(1) GPa resulted in yet another phase transition, leading to the formation of cristobalite X-I (Fig. 4).

The structure model of α-cristobalite was refined at five pressure points. Integrated peak intensities were fit using the GSE_ADA program, and corrected for DAC absorption, Lorenz and polarization effects. Because of the high incident energy and negligible sample thickness, the sample absorption was ignored. Peaks from exposures at the three different detector positions were scaled and merged together. The resulting lists of peaks with corresponding squares of structure factor amplitudes $|F|^2$ and their standard deviations were used for the structure refinement, carried out with the SHELXL software (Sheldrick 2008).

The structure of cristobalite-II was solved by means of the ab initio simulated annealing approach, as implemented in the software Endeavour (Putz et al. 1999; Brandenburg and Putz 2009). The structure model was then refined at each of the three pressure points using the SHELXL program. Because of the limited number of observations, all structure refinements were done using isotopic thermal displacement parameters.

---

[1] It should be noted that at least at ambient pressure only the high-temperature β-cristobalite is a stable phase according to the thermodynamic definition. All other cristobalite phases are metastable. Throughout this paper, we use the term "metastable overpressurization" to describe the phenomenon of suppression of a displacive phase transition from one metastable phase to another that would otherwise occur on compression at ambient temperature.

Fig. 2 Experiment S1: Single-crystal diffraction patterns of α-cristobalite in the ambient temperature stability field at 0.6(1) GPa and in the metastably overpressurized region at 9.1(1) GPa. The three images at each pressure point correspond to the three different detector positions used for data collection. *Black squares* show positions of observed peaks, while the labels above the *squares* indicate the Miller indices of peaks
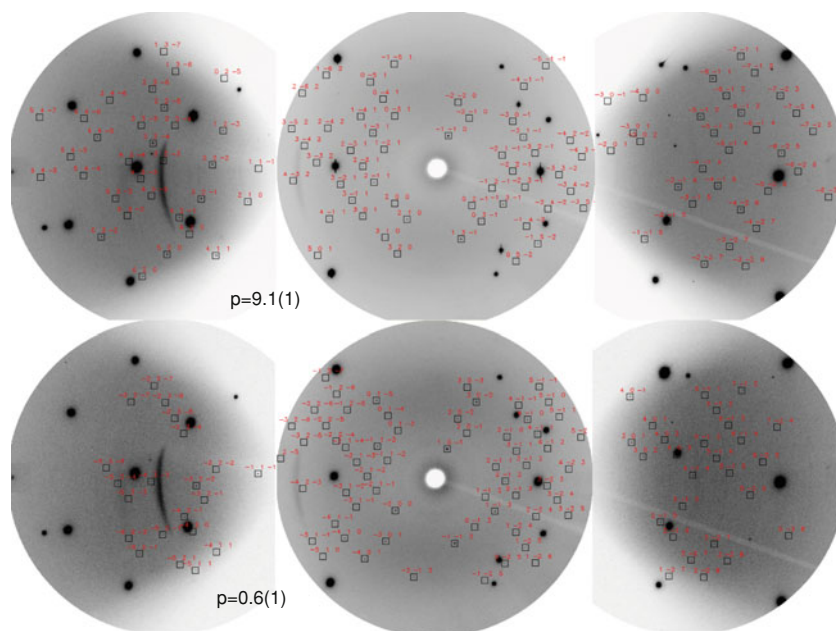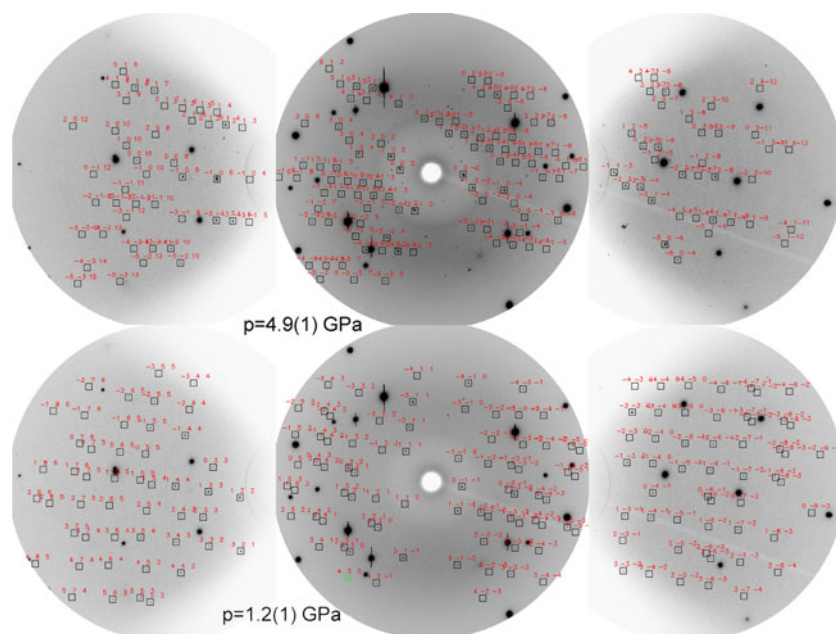

Fig. 3 Experiment S2: Single-crystal diffraction patterns of α-cristobalite at 1.2(1) GPa and cristobalite-II at 4.9(1) GPa. Above the transition, the crystal splits into two components that can be assigned individual orientation matrices


Discussion

Pressure evolution of unit cell parameters and equation of state

Downs and Palmer (1994) elucidated the compressibility and compression mechanism of the α phase up to the transition pressure of 1.6 GPa. Palmer and Finger (1994) characterized the α → II phase transition by measuring the unit cell parameters of cristobalite-II up to the pressure of 4.37 GPa using energy-dispersive powder diffraction in a diamond anvil cell. Onodera et al. (1997) measured the pressure evolution of the unit cell parameters of cristobalite-II in a large volume press experiment with a polycrystalline sample to 3 GPa at room temperature and high temperature. The results of our measurements are in excellent agreement with earlier DAC studies (Downs and Palmer 1994; Palmer and Finger 1994); however, some discrepancies with the large volume press results (Onodera et al. 1997), especially in the values of individual unit cell parameters, should be noted.

The equation of state (EOS) parameters for α-cristobalite have been refined using the third-order Birch-Murnaghan (BM) equation with the unit cell volume fixed to the earlier

Fig. 4 Experiment S2: Single-crystal diffraction patterns of cristobalite-II at 10.1(1) GPa and cristobalite X-I at 12.9(1) GPa. Both below and above the transition, two crystallites with different orientations are present

p=12.9(1) GPa

p=10.1(1) GPa
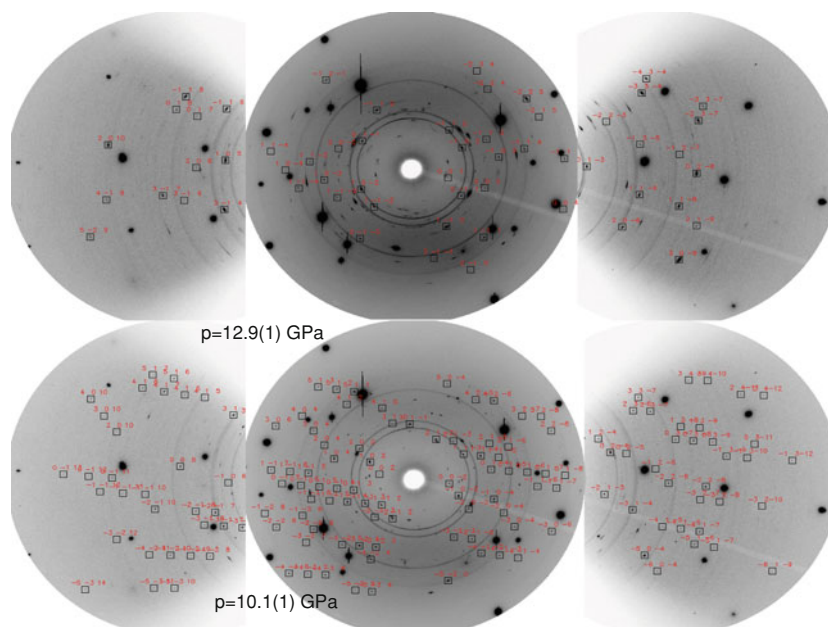
reported value (Downs and Palmer 1994) of $V_0 = 171.42$ Å^3. The values of bulk moduli obtained from our data are $K_0 = 11.0(4)$ GPa and $K' = 8.4(5)$. These values compare very well with the bulk moduli of $K_0 = 11.5(7)$ GPa and $K' = 9(2)$ determined by Downs and Palmer (1994) but are more accurate because of the wider pressure range of the data.

For cristobalite-II, the three pressure points obtained in our experiments were not sufficient to constrain the EOS well; therefore, we merged our data with the results of Palmer and Finger (1994) for the purpose of EOS fitting. This approach seemed justified as both experiments used samples from the same source, and the experimental data showed excellent qualitative agreement. The EOS parameters obtained for cristobalite-II are $K_0 = 25(2)$ GPa, with $K' = 4$, and $V_0 = 174(7)$ Å^3. Figure 5 shows the pressure evolution of unit cell volume for phases α and II (for phase-II, the volume is scaled by a factor of ½ to phase α equivalent). The ambient pressure density of cristobalite-II is slightly lower than that of α-cristobalite (the difference is smaller than one standard deviation). The two V(p) curves cross at pressure of about 1.0 GPa, very close to the point of the α → II transition at ambient temperature. The density increase accompanying the transition is minimal, suggesting that the transition has a weak first-order character. The equation of state curves for the two cristobalite phases is presented in Fig. 5 in comparison with earlier experimental results. Numeric values of the unit cell parameters of α-cristobalite at different pressures are listed in Table 1. As indicated in earlier studies (Downs and Palmer 1994; Onodera et al. 1997) in α-cristobalite, the [0 0 1] direction is more compressible than [1 0 0], leading to a pressure-

induced decrease in the *c/a* ratio. Figure 6 shows the pressure evolution of individual unit cell parameters of both phases [for comparison, the unit cells of phases α and II have been converted to the setting proposed by Palmer and Finger (1994)]. Despite the almost negligible effect on the unit cell volume, the α → II transition induces rather dramatic changes in each of the parameters. Numeric values of the unit cell parameters of cristobalite-II at different pressures are listed in Table 2. The individual pressure variations in *a* and *b* are well described by the BM equation. For the *c* and *β* parameters, the curvature at low pressure is too large for the BM function and a quadratic function yields a much better fit. As shown in Fig. 6, the results of Onodera et al. (1997) deviate from the DAC experimental results. This is most likely because of nonhydrostaticity effects, as well as problems with sufficiently constraining the refinement of the low symmetry monoclinic unit cell from a very limited number of observations.

Compression mechanism of α-cristobalite

Thus far, the sole source of experimental information about the compression mechanism of the α phase has been the single-crystal X-ray diffraction DAC study of Downs and Palmer (1994). The difficulty with using this data to understand the phase relations and structural phase transitions occurring at higher pressure is the very limited pressure range over which the trends have been established, which can lead to significant errors associated with extrapolation. Pressure dependencies of the fractional atomic coordinates obtained from the crystal structure refinements conducted at pressure between 0.6(1) GPa

and 9.1(1) GPa are compared with the earlier experimental and theoretical results in Fig. 7, while the values of the fractional atomic coordinates and thermal displacement
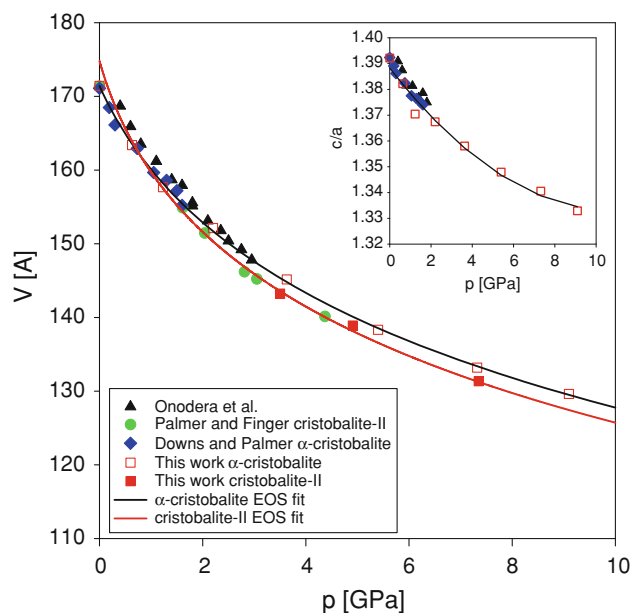

Fig. 5 Pressure evolution of the unit cell volume of α-cristobalite and cristobalite-II. For cristobalite-II, the volume is scaled by ½ to the α-phase equivalent. *Solid lines* show BM EOS fit curves for both phases. The insert shows the pressure evolution of the c/a ratio

Table 1 Unit cell parameters of α-cristobalite as a function of pressure

p[GPa] (ruby)	a[Å]	c[Å]	V[Å³]	c/a
0.00*	4.975(1)	6.9259(8)	171.42(9)	1.3921(4)
0.19*	4.9501(6)	6.8760(6)	168.48(4)	1.3891(2)
0.30*	4.9304(8)	6.8343(8)	166.13(5)	1.3862(2)
0.6(1)	4.908(2)	6.784(4)	163.4(2)	1.382(1)
0.73*	4.9028(8)	6.7782(9)	162.93(6)	1.3825(2)
1.05*	4.8757(8)	6.7163(8)	159.66(6)	1.3775(2)
3.6(1)	4.746(1)	6.445(3)	145.2(1)	1.3580(9)
5.4(1)	4.682(2)	6.311(4)	138.3(2)	1.348(1)
7.3(1)	4.632(2)	6.209(4)	133.2(2)	1.341(1)
9.1(1)	4.599(1)	6.130(3)	129.6(1)	1.3329(9)

Asterisk indicates data from Downs and Palmer (1994)

parameters at different pressures are summarized in Table 3. Structure refinement statistics parameters are listed in Table 4. There is an excellent agreement in the observed trends within the pressure range covered by the earlier study; however, the new results extending to much higher pressure differ from a simple linear extrapolation of the low-pressure data.

The quality of our experimental data does not provide for the direct assessment if the oxygen atoms in α-cristoba-

Fig. 6 Pressure evolution of individual unit cell parameters of α-cristobalite and cristobalite-II, Single crystal results from this study are compared with earlier experimental results of Downs and Palmer (1994), Palmer and Finger (1994) and Onodera et al. (1997). *Solid lines* represent quadratic fit. For cristobalite-II, the EOS fitting was performed with merged data obtained in this study and from Palmer and Finger (1994). For convenience of comparison, the values of parameters are shown in the unit cell setting from Palmer and Finger (1994). The unit cell of α-cristobalite is transformed to this setting by application of transformation matrix [[0.5,0,0],[0,1,0],[0,0,0.5]], whereas the standard unit cell of cristobalite-II used in this paper is transformed to this setting by application of transformation matrix [[1,0,0],[0,1,0],[−0.5,0,0.5]]
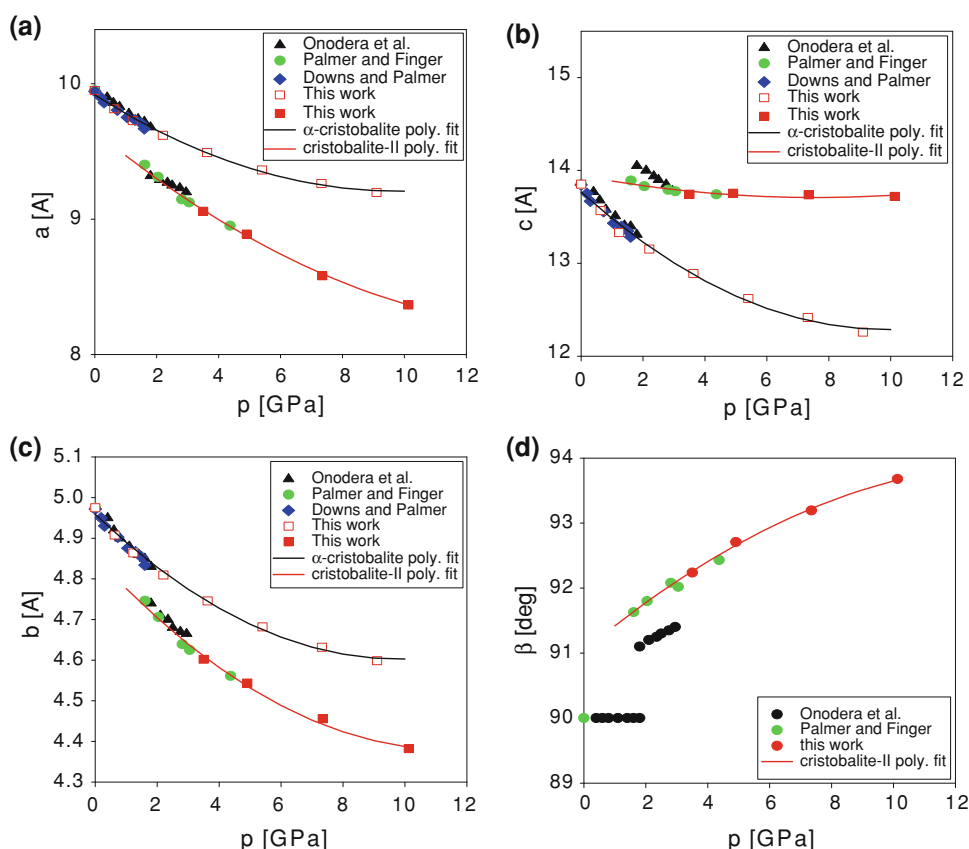
Table 2 Unit cell parameters of cristobalite-II as a function of pressure

p[GPa] (ruby)	a[Å]	b[Å]	c[Å]	β[deg]	V[Å³]
1.61**	8.275(9)	4.746(3)	9.401(9)	122.97(4)	309.7(3)
2.04**	8.214(9)	4.706(3)	9.31(1)	122.71(5)	302.9(3)
2.81**	8.135(9)	4.639(4)	9.15(1)	122.10(6)	292.4(3)
3.05**	8.126(5)	4.625(3)	9.123(8)	122.11(4)	290.4(2)
3.5*	8.082(2)	4.6020(9)	8.905(3)	121.82(1)	286.26(6)
4.37**	8.0399(2)	4.561(1)	8.951(2)	121.36(1)	280.3(5)
4.9(1)	8.011(3)	4.544(3)	8.890(2)	121.0(2)	277.5(9)
7.4(1)	7.894(7)	4.456(5)	8.582(4)	119.7(4)	262(2)
10.1(1)	7.803(6)	4.382(5)	8.366(4)	118.7(4)	251(2)

Asterisk indicates data from Dove et al. (2000). Double asterisk indicates data from Palmer and Finger (1994). The values are given in a standard $P2_1/c$ unit cell setting, different than the one chosen by Dove et al. (2000). The monoclinic unit cell of Dove et al. (2000) can be converted to this setting by application of transformation matrix $[[-1,0,-1],[0,-1,0],[0,0,1]]$

Table 3 Fractional atomic coordinates (numbers in the table are coordinates multiplied by 10^4) and isotropic displacement parameters of α-cristobalite as a function of pressure

p[GPa]	x(Si)	x(O)	y(O)	z(O)	U_{iso}(Si)	U_{iso}(O)
0.00*	3003(1)	2392(2)	1044(2)	1787(1)	9.68(9)	18.74(4)
0.2(1)	3027(4)	2388(8)	1086(9)	1817(5)	10.1(5)	15(1)
0.6(1)	3083(10)	2387(20)	1161(20)	1865(15)	18(2)	12(4)
0.73*	3086(4)	2364(10)	1198(11)	1870(6)	8.0(6)	13(1)
1.05*	3125(5)	2356(15)	1269(15)	1904(8)	6.5(9)	14(1)
3.6(1)	3237(12)	2338(20)	1546(20)	1992(18)	12(3)	10(3)
5.4(1)	3316(15)	2297(30)	1648(30)	2119(16)	9(3)	5(4)
7.3(1)	3353(20)	2276(80)	1768(60)	2228(30)	7(6)	8(8)
9.1(1)	3396(7)	2238(17)	1800(18)	2164(9)	14(2)	11(2)

Si atoms are located on special 4a Wyckofff positions (x, x, 0), while O atoms are at general 8b positions (x, y, z). Asterisk indicates data from Downs and Palmer (1994). U_{iso} are isotropic displacement parameters (Å² × 10³)

Table 4 Statistics of the structure refinement of α-cristobalite at different pressure points

p[GPa]	R_{int}	R_1	wR_2	GooF	Number of unique peaks
0.6(1)	0.083	0.049	0.146	1.27	46
3.6(1)	0.077	0.078	0.184	1.48	39
5.4(1)	0.077	0.074	0.178	1.24	31
7.3(1)	0.330	0.082	0.193	1.46	21
9.1(1)	0.089	0.045	0.109	1.21	37

For dataset at 7.3(1) GPa, the poor crystal centering resulted in a lower quality of intensity data. After elimination of peaks with outlier intensities, the data were still used for refinement and yielded results consistent with the other pressure points. GooF is goodness of fit
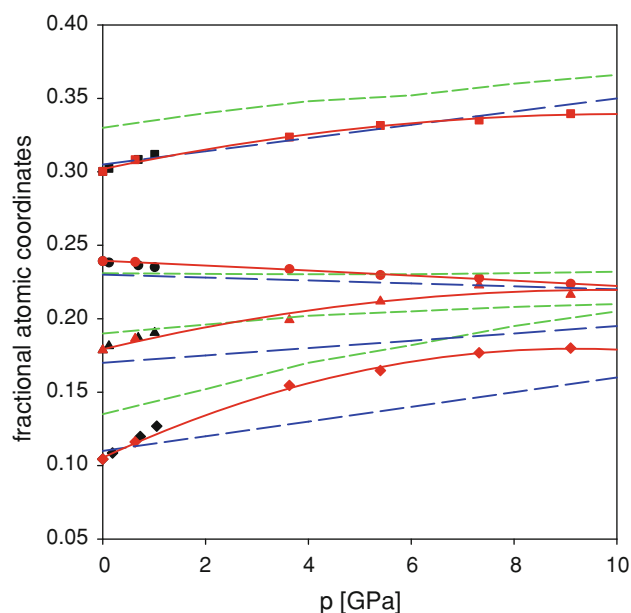

Fig. 7 Pressure evolution of the fractional atomic coordinates of α-cristobalite. Si atoms are located on special 4a Wyckoff positions (x, x, 0), whereas O atoms occupy general 8b position (x, y, z). *Squares* represent x(Si), *circles* x(O), *diamonds* y(O), and *triangles* z(O). *Black symbols* represent earlier measurements of Downs and Palmer. *Red symbols* represent current results. *Dashed lines* show trends determined based on quantum mechanical calculations of Keskar and Chelikowsky (1992) (*green*) and Huang et al. (2006) (*blue*), respectively

lite are fully ordered or partially disordered, like in the β phase. In general, for the silica polymorphs with well-ordered anion sublattices, the ratio of the average isotropic thermal displacement parameters Uiso for Si and O is expected to be 1:2, and our Uiso values fall in that range (Downs et al. 1990).

Over the studied pressure range, the average Si–O bonding distance changes very little, consistent with the Rigid Unit Motion (RUM) model (Dove et al. 2000). However, the slight tendency toward pressure-induced expansion of the bond length, consistent with Si–O–Si angle decrease, seen in the data of Downs and Palmer (1994) is also observed at higher pressure (Table 7). The changes in the crystal structure on compression from 0.6(1) to 9.1(1) GPa are shown in Fig. 8. The main parameter used to describe the compression of tetrahedral SiO₂ phases, which is also the order parameter driving the α–β transition in cristobalite at high temperature, is the variation in the Si–O–Si angle, which reflects the rotation of the tetrahedra. Figure 9 shows the trend observed in our experiments, compared with results of Downs and Palmer (1994) and MD simulations (Garg and Sharma 2007). While there is a good agreement between the experimental data, the classical MD simulations underestimate the tetrahedral rotation.

Quantum mechanical modeling of the compressional behavior of the silica phases is a valuable alternative to difficult experiments; however, reliable simulations in this

Table 5 Changes in the fractional atomic coordinates (numbers in the table are coordinates multiplied by 10^4) of cristobalite-II as a function of pressure

	p = 3.5 GPa*				p = 4.9(1) GPa			
	x	y	z	U_{iso}	x	Y	z	U_{iso}
Si1	6274(11)	2661(16)	8461(9)	18(9)	6265(8)	2742(14)	8472(10)	11(2)
Si2	8660(10)	221(13)	7189(10)	18(9)	8757(8)	79(15)	7218(8)	14(2)
O1	8152(8)	1255(13)	8517(7)	28(6)	8110(19)	1122(40)	8606(20)	15(2)
O2	6944(9)	4046(13)	275(7)	28(6)	6980(30)	4261(60)	33(20)	19(3)
O3	4637(9)	262(10)	7952(8)	28(6)	4636(20)	326(50)	8042(20)	11(2)
O4	696(9)	1948(12)	7604(7)	28(6)	665(30)	1704(50)	7533(30)	16(2)
	p = 7.4(1) GPa				p = 10.1(1) GPa			
	x	y	z	U_{iso}	x	y	z	U_{iso}
Si1	6274(8)	2767(12)	8492(8)	8(2)	6258(19)	2822(50)	8522(30)	10(4)
Si2	8757(6)	9875(16)	7260(6)	11(2)	8769(20)	9612(70)	7287(19)	8(4)
O1	8107(17)	1082(30)	8680(16)	8(2)	823(50)	1155(150)	8780(50)	20(12)
O2	6889(20)	4490(30)	333(20)	17(2)	6839(60)	4673(170)	384(60)	10(10)
O3	4534(20)	338(40)	8043(20)	16(2)	4551(50)	478(140)	8067(70)	18(11)
O4	689(20)	1382(40)	7504(20)	14(2)	670(70)	1033(110)	7402(70)	27(12)

Asterisk indicates data from Dove et al. (2000). The coordinates are given in a standard $P2_1/c$ unit cell setting, different than the one chosen by Dove et al. (2000). The monoclinic unit cell of Dove et al. (2000) can be converted to this setting by application of transformation matrix [[− 1,0, − 1],[0, − 1,0],[0,0,1]]

Fig. 8 Changes in the crystal structure of α-cristobalite on compression from 0.6(1) to 9.1(1) GPa. *Gray tetrahedra* represent the coordination environment of Si. *Gray spheres* represent Si atoms, and *red spheres* represent O atoms
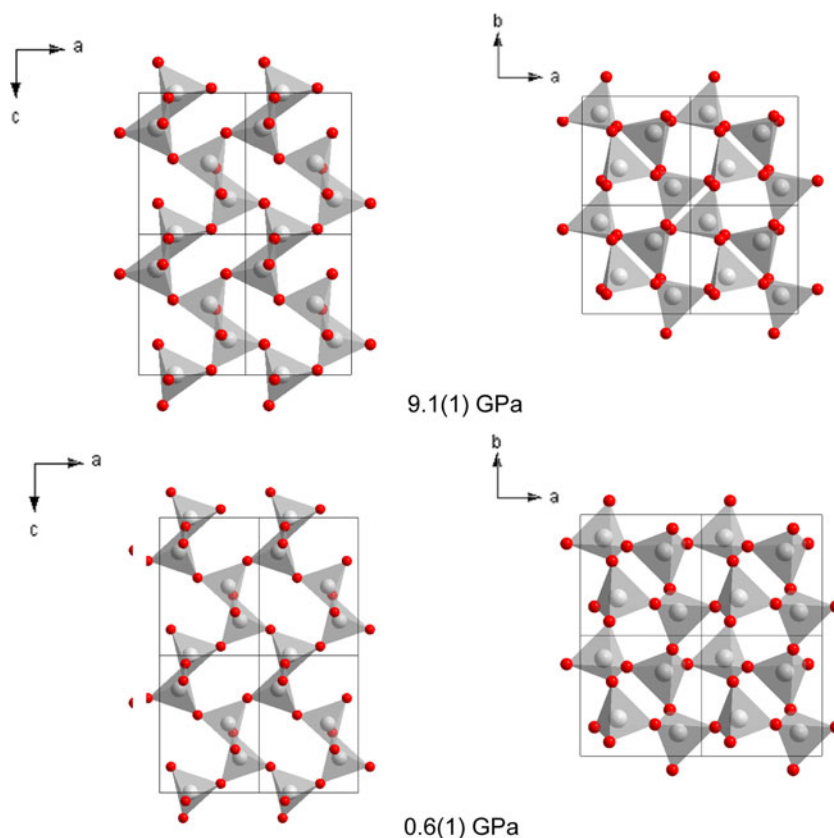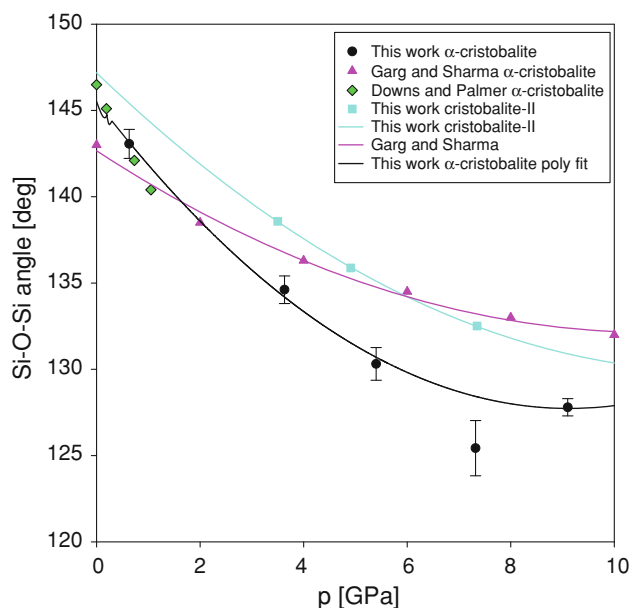
Fig. 9 Pressure-induced changes in the Si–O–Si angle in α-cristobalite and cristobalite-II. Results obtained in this study are compared with earlier experimental results of Downs and Palmer and with classical MD simulations of Garg and Sharma (2007). For α-cristobalite, the data point at 7.3(1) GPa, which has the largest standard deviation, was omitted in the polynomial fit as an outlier

particular chemical system are far from trivial because of the complicated electronic interactions and small differences in the total energy between polymorphs with similar coordination. One of the early quantum mechanical studies that addressed the question of the compression mechanism of α-cristobalite utilized soft pseudopotentials derived with the use of the local density approximation approach (LDA) (Keskar and Chelikowsky 1992) and predicted the pressure evolution of the fractional atomic coordinates. Compression mechanism models were also derived in more recent molecular dynamics simulations (Huang et al. 2006; Liang et al. 2007; Durandurdu 2009). There are two competing interpretations for the molecular dynamics compression

Table 6 Statistics of the structure refinement of cristobalite-II at different pressure points

p[GPa]	R_{int}	R_1	wR_2	GooF	Number of unique peaks
4.9(1)	0.163	0.063	0.170	1.24	131
7.4(1)	0.096	0.069	0.172	0.99	127
10.1(1)	0.104	0.094	0.225	1.61	54

GooF is goodness of fit. At 10.1(1) GPa, the data used for refinement were collected only at two detector positions, resulting in less observations

mechanism simulation results. Liang et al. (2007) favor a compression mechanism involving a trend toward a *bcc* arrangement of oxygen (analogous to the trend observed in quartz, Sowa 1988; Dmitriev et al. 1997; Thompson and Downs 2010), followed by a discontinuous transformation (accompanying the phase transition to the octahedrally coordinated phase) to an *hcp* close-packed structure. On the other hand, Huang et al. (2006) and Durandurdu (2009) predict a continuous tendency toward the *hcp* arrangement within the α-phase. Pair distribution function analysis is a convenient way to qualitatively assess which of these models is more consistent with our data. For that reason, we used the PDFgui program (Farrow et al. 2007) to compute the O–O partial $G(r)$ pair distribution function based on our refined models. The results of this analysis are shown in Fig. 10. It is apparent that the O–O pair distribution function of α-cristobalite simplifies as pressure increases. A rapid pressure-induced decrease in the intertetrahedral O–O distances causes the second $G(r)$ peak to move much closer to the intratetrahedral first peak, but the doublet characteristic of the *bcc* lattice is still far from ideal at 9.1(1) GPa, and instead it is split into a triplet and seems to show a tendency to merge into a single peak which would be indicative of an *hcp* arrangement. The three peaks between 4 and 6 Å are also closer to *hcp* rather than to the *bcc* features. Overall,

Table 7 Selected bond lengths (in Å) and interatomic angles (in deg.) in the structure of α-cristobalite at different pressures

p[GPa]	Si–O × 2	Si–O × 2	Si–O–Si	O–Si–O × 2	O–Si–O × 2	O–Si–O	O–Si–O
0.00*	1.603(1)	1.598(5)	146.49(6)	108.20(2)	109.99(7)	109.03(9)	111.42(8)
0.19*	1.598(5)	1.606(4)	145.1(2)	108.2(1)	109.3(3)	109.6(4)	111.6(3)
0.6(1)	1.59(1)	1.615(9)	143.1(8)	108.2(2)	109.2(6)	110.5(9)	111.5(8)
0.73*	1.600(6)	1.609(5)	142.1(3)	108.0(1)	109.9(3)	109.6(4)	111.6(4)
1.05*	1.602(8)	1.610(6)	140.4(4)	107.8(2)	109.8(4)	110.0(5)	111.6(5)
3.6(1)	1.57(1)	1.63(1)	134.6(8)	106.4(3)	109.9(6)	111.4(8)	112(1)
5.4(1)	1.62(2)	1.62(1)	130(1)	107.3(4)	108.9(8)	112(1)	113(1)
7.3(1)	1.62(3)	1.64(3)	125(2)	107.2(9)	108(2)	111(3)	116(2)
9.1(1)	1.61(1)	1.62(1)	127.8(5)	106.2(2)	110.1(5)	111.7(6)	112.0(7)

Asterisk indicates data from Downs and Palmer (1994)

Fig. 10 Partial O–O G(r) pair distribution function computed for the compression of cristobalite-II (**a**) and α-cristobalite (**b**) compared with the ideal body-centered cubic (*bcc*) and hexagonal close-packed (*hcp*) structure G(r) functions (**c**). For reference, a G(r) for quartz at 20 GPa (very close to ideal *bcc*) is also shown (**c**)
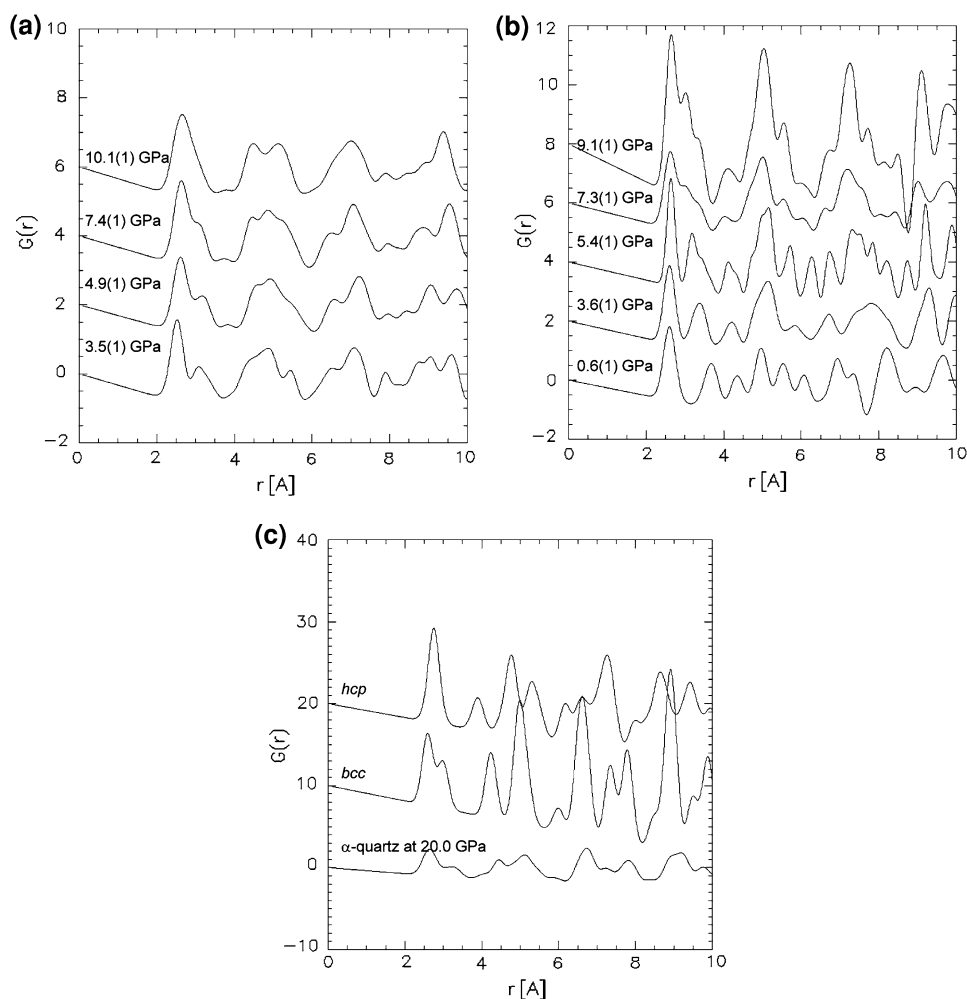
the $G(r)$ trend for α-cristobalite does not clearly favor either the *bcc* or *hcp* tendency.

Compression mechanism of cristobalite-II

Despite the fact that the occurrence of the $\alpha \rightarrow$ II transition has been confirmed in multiple experimental studies, to the best of our knowledge, the compression mechanism of cristobalite-II has not been subject of quantum mechanical simulations other than the ones reported in the original study that introduced the structure model (Dove et al. 2000).

Our results fully confirm the validity of the cristobalite-II structure proposed by Dove et al. (2000). The values of the fractional atomic coordinates of cristobalite-II at different pressures are summarized in Table 5, while structure refinement statistics parameters are listed in Table 6. The $\alpha \rightarrow$ II transformation has little effect on the Si–O bond length, again in agreement with the RUM-based mechanism (Table 8). The average Si–O–Si angle at the transition drops discontinuously by about 3°, compared to that in the

α-phase. The general trend for pressure variation in the Si–O–Si angle is decreasing but has a smaller slope than in the α-phase. The structure models of cristobalite-II at 4.9(1) and 10.1(1) GPa are compared in Fig. 11.

Just like in the case of α-cristobalite, it seems justified to expect that the atomic rearrangements accompanying the compression of cristobalite-II should reflect a trend toward assuming a higher-symmetry ideal geometry of the anion sublattice. As discussed above, the trend we observed for overpressurized α-cristobalite leads toward an arrangement intermediate between *hcp* and *bcc*. The $\alpha \rightarrow$ II transformation results in some rather dramatic changes in the $G(r)$, which immediately, at pressure of only 1.8 GPa, starts to closely resemble the *bcc* arrangement, despite the low symmetry of phase-II, as shown in Fig. 10. As pressure increases, $G(r)$ clearly evolves into a shape characteristic of the close-packed structure. At 10.1(1) GPa, the first $G(r)$ peak is already single and is followed by a broad doublet, as expected for the *bcc* arrangement. This way the $\alpha \rightarrow$ II transformation acts as a

Fig. 11 Changes in the crystal structure of cristobalite-II on compression from 4.9(1) to 10.1(1) GPa. *Gray tetrahedra* represent the coordination environment of Si. *Gray spheres* represent Si atoms, and *red spheres* represent O atoms
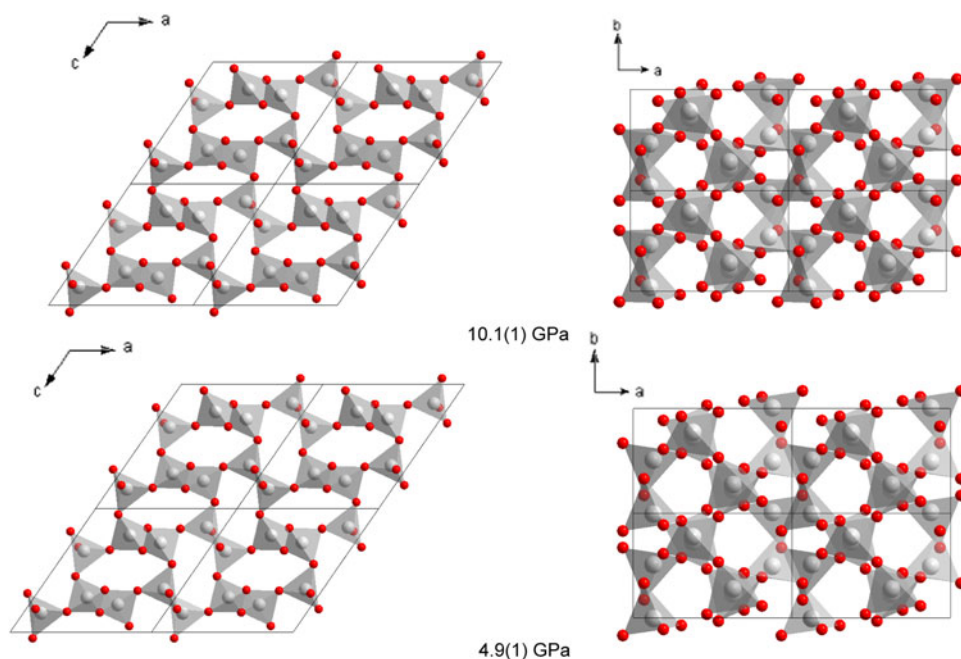

Table 8 Tetrahedral Si–O bond lengths (in Å) in the structure of cristobalite-II at different pressures

p[GPa]	3.5 GPa*	4.9 GPa	7.4 GPa	10.1(1) GPa
Si1-O1	1.626(9)	1.57(1)	1.58(2)	1.57(7)
Si1-O2	1.569(9)	1.58(3)	1.59(2)	1.61(8)
Si1-O3	1.59(1)	1.59(2)	1.605(8)	1.61(4)
Si1-O3	1.619(9)	1.64(2)	1.63(2)	1.64(5)
Si2-O1	1.537(8)	1.57(1)	1.56(2)	1.57(6)
Si2-O2	1.583(8)	1.59(2)	1.602(8)	1.62(5)
Si2-O4	1.681(9)	1.58(3)	1.62(1)	1.62(6)
Si2-O4	1.572(8)	1.64(2)	1.63(2)	1.64(7)

Asterisk indicates data from Dove et al. (2000)

vehicle to transform the oxygen sublattice into a more ideal *bcc* arrangement and at the same time opens an avenue toward assuming the close-packed O-substructure.

Cristobalite-II → cristobalite X-I transition

The II → X-I transition has also been consistently observed in several independent experimental studies, but to the best of our knowledge, sufficiently good quality diffraction data that can provide an unambiguous structure solution have never been obtained for phase X-I. Recent quantum mechanical simulations seem to strongly favor the idea that cristobalite X-I should be isosymmetric with α-cristobalite, or be an orthorhombic distortion ($C222_1$) of the ambient phase (Huang et al. 2006; Liang et al. 2007; Donadio et al. 2008; Durandurdu 2009). Indeed, some rather qualitative agreement between the observed and calculated diffraction

peak *d*-spacings has been noted; however, most recent powder experiments (Dubrovinsky et al. 2004) seem to indicate that the symmetry of phase X-I is monoclinic.

The diffraction patterns of cristobalite X-I observed in our experiment S_2 at 12.9(1) GPa (Fig. 4) show some signs of degraded quality of the transformed single-crystal specimens, but nevertheless include as many as 60 peaks corresponding to each of the three samples (because of the very small size of the focused incident beam, the diffraction patterns from each crystal are collected separately), and can be easily indexed. Data with this information content provide a significant improvement in reliability of the unit cell and space group determination, compared to the previous powder diffraction results in which indexing was based only on a few peaks and the information is purely one dimensional (reciprocal space vector lengths in powder experiment, versus three-dimensional Cartesian coordinates of each vector in the single-crystal experiment). Indexing of the patterns from all three crystals yields the same primitive monoclinic unit cell with $a = 5.582(6)$ Å, $b = 4.092(5)$ Å, $c = 6.853(2)$ Å, $β = 98.31(3)°$, while systematic absences indicate that the most likely space group is $P2_1/c$ or $P2_1/n$, with $Z = 6$ and density of 3.29 g/cm^3. This unit cell is different from the one proposed by Dubrovinsky et al. (2004). The fact that the calculated density for cristobalite X-I suggests almost no volume discontinuity on II → X-I transition is consistent with the molecular dynamics simulations and strongly supports the notion that there is no change in the coordination number (in contrast to the mixed-coordination model proposed by Dubrovinsky et al. 2004), as also indicated by IR measurements (Yahagi et al. 1994). Because of the lower quality of

the peak intensity data resulting from peak broadening accompanying the II → X-I transition, we have not yet been able to solve the structure of cristobalite X-I, but the reliable information about the unit cell parameters, space group, and unit cell contents can hopefully be used by theorists to compute plausible models that could then be verified for consistency with our experimental data.

Summary and conclusions

The experimental realization of the theoretically predicted high compression rate-induced metastable suppression of the displacive $\alpha \rightarrow$ II transition allowed us to obtain valuable information about the compression mechanism of α-cristobalite well beyond its ambient pressure stability field. In its thermodynamic nature, this intriguing phenomenon is similar to supercooling. As pressure increases the structural dissimilarity between the two polymorphs, there is a concomitant increase in the associated activation barrier of the transformation. To the best of our knowledge, an analogous phenomenon involving a displacive phase transition has not been observed before with comparable clarity and reliability, but it is possible that it can be expected in other crystalline systems characterized by phase space energy landscapes similar to SiO_2.

While the two experiments described above were performed in different pressure media (alcohol mixture and Ne), we can clearly rule out the possibility that the medium choice played the controlling role in the suppression of the transformation to phase-II. The experiments of Downs and Palmer (1994) performed in alcohol pressure medium (the same as in our experiment S_1) demonstrate that both types of behavior can be obtained in alcohol. To verify the same hypothesis for Ne, we also performed additional single-crystal experiment with Ne pressure medium in which cristobalite-II was successfully observed (also by means of synchrotron single-crystal diffraction) at 2.2 GPa.

While we infer that the factor controlling the suppression of the $\alpha \rightarrow$ II transition is the rate of compression, our experiments do not address directly the issue of the threshold rate (or timescale) required to induce the suppression phenomenon. Instead, the parameter that we were able to control [similarly like in the simulations of Garg and Sharma (2007)] was the magnitude of the pressure increase. In a standard screw-driven DAC, individual pressure increase steps occur on a time scale of perhaps 0.1 s (during this time, pressure increases to approximately 90% of the final value), while complete equilibration requires time as long as 15–30 min. We estimated that the compression rate reached in experiment S_1 was ∼50 GPa/s. Proper quantification of this threshold will definitely require further experiments but should be possible because of the reversible character of the transition.

The unambiguous determination of the crystal structure of the unquenchable high-pressure phase-II (consistent with the model of Dove et al. (2000)), based on single-crystal X-ray diffraction data confirms that this phase needs to be seriously considered in quantum mechanical simulations that model the densification process of silica. The pressure-induced variations in the structure model of cristobalite-II indicate that the $\alpha \rightarrow$ II transformation allows the cristobalite structure to immediately assume a more ideal close-packed oxygen sublattice arrangement. Unlike in α-cristobalite, the pressure-induced changes in the $G(r)$ of phase-II show a very clear trend toward assuming a close-packed O-substructure needed to facilitate the transformation to the octahedrally coordinated phases. These observations imply that the ab initio models appear to fail because of inadequate modeling of non-bonded O–O interactions.

Because of the limitation of the hydrostatic range of the alcohol pressure medium, our experiment with the over-pressurized α-cristobalite did not reach the pressure at which the formation of phase X-I is normally observed. It will, however, be very interesting to see what the effect of the preservation of the α-phase is. One may speculate that in this case, a different transformation route to the octahedral phases might be followed.

The preliminary three-dimensional single-crystal data obtained for cristobalite X-I clearly show that the unit cell for this phase is not tetragonal, as favored by the MD simulations, and is different than the unit cell proposed on the basis of the recent powder diffraction experiments. While the structure model for this phase still remains elusive, the new experimental constraints should aid the theoretical efforts to reveal the true nature of this phase.

References

Brandenburg K, Putz H (2009) Endeavour. Crystal Impact GbR, Bonn

Dera P (2007) GSE_ADA data analysis program for monochromatic single crystal diffraction with area detector. GSECARS, Chicago

Dewaele A, Datchi F et al (2008) High pressure-high temperature equations of state of neon and diamond. Phys Rev B77:094106

Dmitriev V, Torgashev V et al (1997) Theory of SiO_2 polymorphs. Europhys Lett 37:553–558

Donadio D, Martonak R et al (2008) Influence of temperature and anisotropic pressure on the phase transition in a-cristobalite. Phys Rev Lett 100:165502

Dove MT, Craig MS et al (2000) Crystal structure of the high-pressure monoclinic phase-II of cristobalite, SiO_2. Mineral Mag 64:569–576

Downs RT, Palmer DC (1994) The pressure behavior of a cristobalite. Am Mineral 79:9–14

Downs RT, Gibbs GV et al (1990) A study of the mean-square displacement amplitudes of Si, Al and O atoms in framework structures: evidence for rigid bonds, order, twinning and stacking faults. Am Mineral 75:1253–1267

Dubrovinsky LS, Dubrovinskaia NA et al (2004) A class of new high-pressure silica polymorphs. Phys Earth Planet Inter 143–144:231–240

Durandurdu M (2009) Formation of an anataselike phase in silica under anisotropic stress: an ab initio constant-pressure study. Phys Rev B 80:024102

Farrow CL, Juhas P et al (2007) PDFfit2 and PDFgui: computer programs for studying nanostructure in crystals. J Phys Condens Matter 19:335219

Garg N, Sharma SM (2007) Classical molecular dynamical simulations of high-pressure behavior of alpha cristobalite (SiO_2). J Phys Condens Matter 19:456201

Huang L, Durandurdu M et al (2006) Transformation pathways of silica under high pressure. Nat Mater 5:977–981

Keskar NR, Chelikowsky JR (1992) Structural properties of nine silica polymorphs. Phys Rev B46:1–13

Klotz S, Chervin J-C et al (2009) Hydrostatic limits of 11 pressure transmitting media. J Phys D Appl Phys 42:075413

Liang Y, Miranda CR et al (2007) Tuning oxygen packing in silica by nonhydrostatic pressure. Phys Rev Lett 99:215504

Mao HK, Xu J et al (1986) Calibration of the ruby pressure gauge to 800 kbar under quasi-hydrostatic conditions. J Geophys Res 91:4673–4676

Onodera A, Suito K et al (1997) Synchroteon X-ray diffraction study of cristobalite at high pressure and high temperature. High Pressure Res 15:307–319

Palmer DC, Finger LW (1994) Pressure-induced phase transition in cristobalite: an X-ray powder diffraction study to 4.4 GPa. Amer Mineral 79:1–8

Palmer DC, Hemley RJ et al (1994) Raman spectroscopic study of high-pressure phase transitions in cristobalite. Phys Chem Mineral 21:481–488

Putz H, Schon JC et al (1999) Combined method for 'Ab Initio' structure solution from powder diffraction data. J Appl Cryst 32:864–870

Rivers ML, Prakapenka VB et al (2008) The COMPRES/GSECARS gas loading system for diamond anvil cells at the advanced photon source. High Pressure Res 28:273–292

Sheldrick GM (2008) A short history of SHELX. Acta Cryst A64:112–122

Sowa H (1988) The O packings of low-quartz and ReO3 under high pressure. Zeit Krist 184:257–268

Thompson RM, Downs RT (2010) Packing systematics of the silica polymorphs: the role played by O–O nonbonded interactions in the compression of quartz. Am Mineral 95:104–111

Tsenyuki S, Matsui Y et al (1989) New pressure-induced structural transformations in silica obtained by computer simulation. Nature 339:209–211

Van Valkenburg A, Buie BF (1945) Octahedral cristobalite with quartz paramorphs from Ellora Caves, Hyderabad State, India. Am Mineral 30:526–535

Yahagi Y, Yagi T et al (1994) Infrared absorption spectra of the high-pressure phases of cristobalite and their coordination numbers of silicon atoms. Solid State Comm 89:945–948